

Micro and nanoparticulate PP/CaCO₃ composites mechanical, thermal and transport properties - DOE*

Juliano Martins Barbosa^{1,2*} , Caroline Valadão Pacheco¹ , Gisele Szilágyi¹ ,
Patrícia Candioto de Oliveira¹ , Renato Meneghetti Peres¹  and Hélio Ribeiro¹ 

¹*Departamento de Engenharia de Materiais, Escola de Engenharia, Universidade Presbiteriana Mackenzie, São Paulo, SP, Brasil*

²*Programa de Pós-graduação em Ciência e Engenharia de Materiais - PPGCEM, Departamento de Engenharia de Materiais – DEMa, Universidade Federal de São Carlos - UFSCar, São Carlos, SP, Brasil*

**barbosa_jm@yahoo.com.br*

**This paper has been partially presented at the 17th Brazilian Polymer Congress, held in Joinville, SC, 29/Oct - 02/Nov/2023.*

Abstract

Composite based on PP/CaCO₃ contained micro and nanoparticles were investigated in relation its activation volume, mechanical, thermal and transport properties. The additives were initially dispersed in homopolymer polypropylene (hPP) blended with compatibilizer maleic anhydride grafted polypropylene (PP-g-MA) in twin-screw extruder, producing CaCO₃ masterbatches, that were subsequently diluted in hPP. To optimize fillers dispersion in the polymer matrix, a Design of Experiment (DOE) was used, that combined Extruder screw rotation (N: 250 and 500 rpm); Extruder feed flow (Q: 10 and 15 kg/h) and Average particle size (ϕ : 40 nm and 1.7 μ m) at four different filler concentrations. Based on mechanical characterization results, the best process found was 500 rpm@10 kg/h, which provided suitable Specific Mechanical Energy (SME), increasing the nanocomposites strength. Finally, improvements of Impact Resistance up to 7.8% and Young's Modulus up to 9.3% related to microcomposite and Tensile Strength (F_{max}), up to 7.9%, related to hPP, with higher strain.

Keywords: *activation volume, calcium carbonate, design of experiment, mineral fillers, nanocomposites.*

How to cite: Barbosa, J. M., Pacheco, C. V., Szilágyi, G., Oliveira, P. C., Peres, R. M., & Ribeiro, H. (2024). Micro and nanoparticulate PP/CaCO₃ composites mechanical, thermal and transport properties - DOE. *Polímeros: Ciência e Tecnologia*, 35(1), e20250003. <https://doi.org/10.1590/0104-1428.20240071>

1. Introduction

Polymers have been filled with various materials to enhance different properties such as thermal, mechanical, electrical, or transport properties^[1-3]. In this context, inorganic mineral fillers like talc, mica, silica, and calcium carbonate are commonly, also have been used in different proportions added to the polymeric matrix^[4], owing to their varied aspect ratio and interfacial interactions^[5]. These fillers interactions have been studied to seek improvements since macroscopic reinforcing elements typically have imperfections. Therefore, smaller reinforcing elements, even reaching the nanometric scale, are sought to reduce these imperfections in desired materials^[6]. One of the most commonly used mineral fillers is CaCO₃, available in natural or synthetic forms^[7]. Micrometric particles are typically selected using sieves, while the nanometric are prepared using various techniques, such as physical vapor deposition, chemical vapor deposition, reactive precipitation, sol-gel, and microemulsion methods^[8], among these, industrial reactive precipitation is of particular interest^[8]. Additionally,

the shape of the particles also influences its properties when used in composites. For instance, using spherical or elongated nanoparticles can influence their physical and chemical properties differently, due to its distinct aspect ratios^[4]. Typically, the electrical, mechanical and thermal properties obtained from nanocomposites usually are superior to the microcomposites, without affect the polymer processability^[8,9]. Additionally, dispersing nanoparticles in a polymeric matrix can create new levels of interaction, not present in microparticle systems, leading to changes their features and improvements in its physical properties. Nanocomposite processing can be achieved using various techniques including in-situ polymerization, melt mixing, and the sol-gel process, among others, each with its own advantages and disadvantages^[8]. To enhance dispersion during the melt mixing process, one option is to modify the surface of the nanoparticles^[10] This strategy can prevent agglomeration, improves dispersion quality, and enhances adhesion with the polymeric matrix. Usually, nanoparticles are treated with surfactants or organic agents, like those used in conventional composites. Although these agents

can improve filler dispersion, they may not always facilitate strong adhesion between components, leading to limited interaction and short-distance bonding in nanocomposites, mainly in thermoplastic polymers^[9]. Alternatively, adjusting the process itself can be considered. It's worth noting that smaller particles have a larger surface area, increasing the system's surface energy and promoting enhanced interaction between components^[11]. Dispersing particles without modification is difficult as they tend to aggregate. Hence, efficient shear processes with Specific Mechanical Energy (SME) are crucial for nanoparticle dispersion^[12,13]. The SME can be modulated during extrusion by adjusting the extruder screw rotation (N) and extruder feed flow (Q), aiding in better filler dispersion, and breaking up the aggregates^[14]. Rocha et al.^[15] investigated this phenomenon, by the influence of twin-screw extruder rotation on incorporating various CaCO₃ nanoparticles into hPP, resulting in a significant increase in flexural strength without compromising impact resistance. Similarly, Thio et al.^[16] examined the impact of CaCO₃ particle size on PP mechanical properties. They analyzed three CaCO₃ types sized at 0.07, 0.7, and 3.5 μm, dispersed in PP at concentrations from 0.05 to 0.30 wt%. With low filler levels, Young's Modulus increased, and tensile strength decreased regardless of filler size. Impact resistance improved with filler content until a critical concentration. Notably, the 0.7 μm filler increased composite impact resistance by fourfold compared to unfilled PP at a 5wt%^[16]. Chan et al.^[17] investigated the addition of CaCO₃ nanoparticles (44,0 nm) into hPP via a twin-screw extruder at various concentrations, observing an increase in the composite's impact resistance. Zhang et al.^[18] fabricated PP/CaCO₃ nanocomposites using a twin-screw extruder, integrating a small amount of non-ionic modifier (poly-oxyethylene noni-phenol) during extrusion to enhance compatibility between filler and the polymer matrix. Considering the properties of CaCO₃ nanoparticles, there is potential for its utilization in several materials, such as: plastics, rubbers, paints and other natural or synthetic materials, as reinforcement or additives^[3,19]. For example, its addition in PP can raise both impact resistance and Young's modulus at the same time^[19]. Thus, this study focused on crafting PP/CaCO₃ composites using a PP-g-MA compatibilizer agent and employing a Design of Experiment (DOE)^[20,21]. In this case, the processing was used in two stages: initially preparing the *masterbatches* followed by different dilutions steps. Essential tests were conducted at each stage to evaluate the properties of interest^[22,23].

2. Materials and Methods

The study unfolded in two phases: First involved designing experiments (DOE) to prepare and dilute the concentrates,

while second, it was focused on characterizing micro and nanocomposites. Initially, a concentrate was created using a co-rotational twin-screw extruder, employing DOE and adjusting shear levels via SME, varying extrusion parameters such as extruder screw rotation (N) and feed flow (Q) to modulate it. Subsequently, dilutions of each concentrate were conducted to produce micro and nanocomposites, which were characterized to evaluate mechanical, thermal, and transportation properties. The used nanoparticulate precipitated of CaCO₃ NPCC-201 (D₅₀: 40 nm, surface area: 40 m²/g, purity > 94.5% treated with fatty acid), was manufactured by *NanoMaterial Technology Pte Ltd* – Singapore^[24] and Microparticulate CaCO₃ Omyacarb 1T-AV (D₅₀: 1.6 to 1.7 μm, purity > 97.3%, also treated with fatty acid), was manufactured by *Omya International AG - Italy*^[25]. Compatibilizer maleic anhydride grafted polypropylene (PP-g-MA) - Fusabond P MD353D (MFI: 450 g/10min - 2.16 kg@190 °C, MP: 136 °C and maleic anhydride concentration > 1,0%), were supplied by *DOW Inc*^[26]. Polypropylene (PP) homopolymer, H301 (MFI: 10 g/10min - 2.16 kg@230 °C), was supplied by *Braskem S/A*^[27]. The Desig of Experiment (DOE) combined three variables at two levels: Extruder screw rotation (N: 250 and 500 rpm), Extruder feed flow (Q: 10 and 15 kg/h) and D₅₀ (φ: 40nm and 1.7μm). The samples were identified according to the methodology shown in Figure 1 below^[22]. Combining the variables, it was obtained eight processing conditions, as shown in Table 1.

To prepare the concentrates (*masterbatches*), it was used 20% of CaCO₃ (micro or nanoparticulate), 70% hPP, and 10% PP-g-MA, processed in a co-rotational twin-screw extruder (ZSK18 *Coperion GmbH*, D: 18 mm, L/D: 48, power of 4 kW /5.43 hp, max amperage of 15.2 A, max screw rotation of 600 rpm, and a max feed rate of 140 kg/h) using the main feeder (without side feeder). The thermal profile ranged from 140 to 180 °C, and the extruder screw profile was based on the scheme shown in Figure 2^[28], with adaptations due to differences in the L/D of the extruders.

The concentrates previously prepared were diluted in hPP using the same twin-screw extruder (Temp.: 140–180°C, N: 500 rpm, Q: 10 kg/h). Dilutions were carried out at four dosages for each concentrate: 2.5%, 7.5%, 25.0%, and 50.0%. Consequently, the CaCO₃ content in each composite depended on the proportion added to hPP, calculated as the dosage multiplied by the CaCO₃ content in the concentrate, resulting in 0.5%, 1.5%, 5.0%, and 10.0%. These values were used to identify each composite. In relation to the MFI (Melt Flow Index) of hPP, it was obtained a value of 10.8 g/10 min (2.16 kg@230 °C). Due to the very low viscosity of PP-g-MA, its exact value could not be accurately determined, but it was detected to be >200 g/10 min under

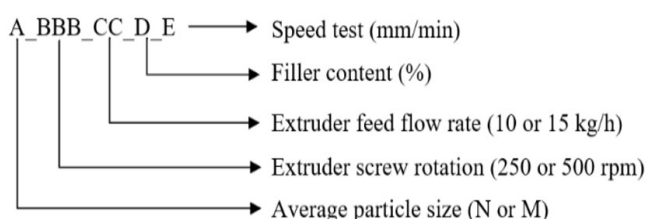
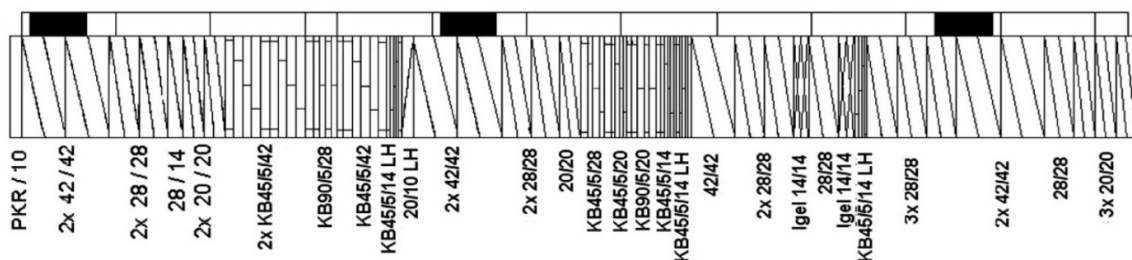


Figure 1. Methodology for identifying samples.

Table 1. Process conditions for the concentrates.

Run	Sample	Screw rotation N (rpm)	Feed flow Q (kg/h)	Particle size ϕ (μm)
Concentrate 1	N_250_10	250	10	0.04
Concentrate 2	M_250_10	250	10	1.70
Concentrate 3	N_250_15	250	15	0.04
Concentrate 4	M_250_15	250	15	1.70
Concentrate 5	N_500_10	500	10	0.04
Concentrate 6	M_500_10	500	10	1.70
Concentrate 7	N_500_15	500	15	0.04
Concentrate 8	M_500_15	500	15	1.70


Figure 2. Diagram of the screw profile used in processing.

the same conditions. The ash content (inorganic part) of masterbatches samples were conducted in triplicate, and the values are shown in Table 2. To determine the crystallinity degree of the concentrates, each peak area, along with the amorphous halo (Ac + Aa), was calculated, generating a sum of the areas. This determination was performed using the *Origin Pro8* program with the *Fit Multi-peaks* tool, applying the *Lorentzian* peak function. After establishing a baseline to eliminate the amorphous halo, the same peaks areas were measured again (Ac).

2.1. Characterization

For the CaCO₃ particles morphological characterization was used Scanning Electron Microscopy (SEM) on the Zeiss-Supra 35 equipment. The average particle sizes of CaCO₃ micro and nanoparticles were characterized with size measurements conducted via *Image J* software. X-ray Diffraction (WADX) on the Rigaku DMax 2500 PC equipment (radiation source: CuK α , λ : 1.54056 Å, scan at 2 θ : 5 to 75°). The surface area (BET) was determined by the Micromeritics Instrument Corporation model ASAP 2000 V3.03 A, with a N₂ atmosphere. For the polymers, hPP and PP-g-MA. The MFI^[29] was determined using the Aflo Extrusion Plastometer (ZwickRoell GmbH & Co) at 2.16 kg@230 °C. For concentrate characterization, the Ash Content^[30] was determined by heating until constant mass in an oven (600 °C). Additionally, X-ray Diffraction (with a CuK α radiation source, λ : 1.54056 Å, scan at 2 θ : 1 to 30°) was used to determine the crystallinity degree. The composite specimens were molded by injection molding in the Romi Primax 65R equipment (Injection temperature: 200 °C@70 bar, mold: 23±2 °C@35 s). Tensile tests were executed on the Universal Testing Machine (Z100-100 kN equipment) from ZwickRoell GmbH & Co. To determine the Young's modulus, tensile strength and elongation of the composites, it was used the following parameters (load cell:

5KN; deformation speeds: 50 mm/min)^[31]. The Activation Volume was determined by the Eyring equation, that is associated with mobility at the organic-inorganic interface, specifically the polymer-filler interface. Therefore, the smaller the activation volume of the composite, the greater the restriction on the mobility of chain segments at the polymer-filler interface, indicating stronger interaction. This model is represented in Equation 1^[32].

$$\sigma \cong \frac{A}{V} + \frac{RT}{V} \times \ln \left(\frac{V}{V_0} \right) \quad (1)$$

$$\alpha = \frac{RT}{V} \quad (2)$$

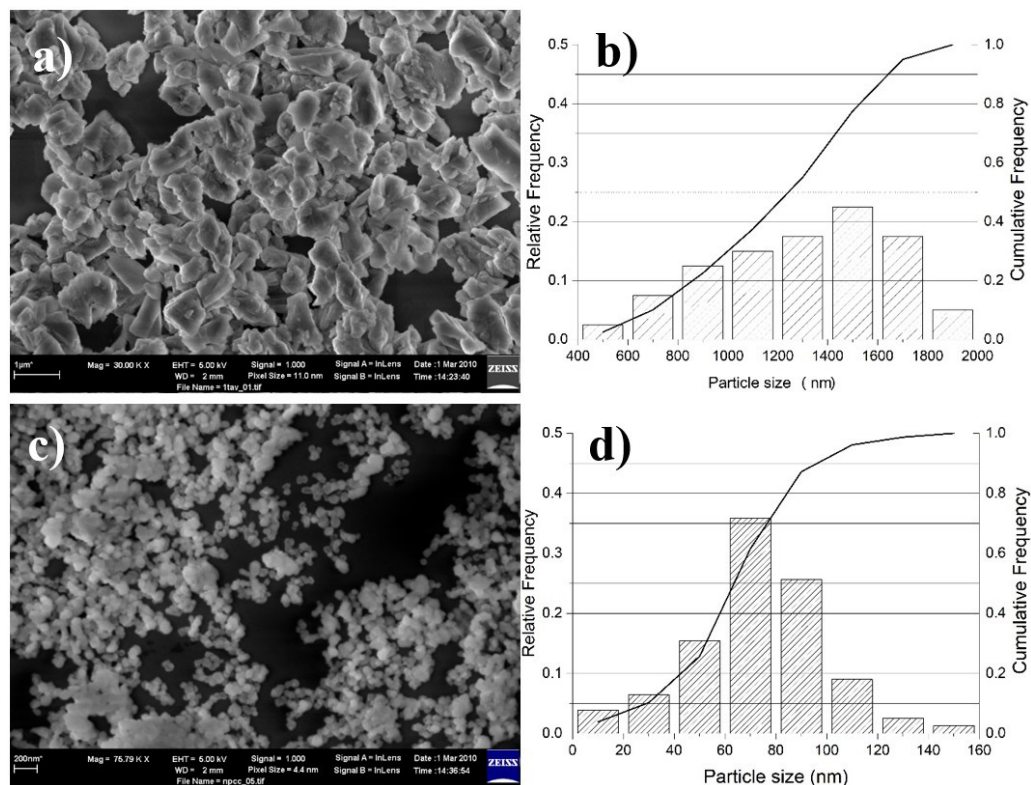
Where σ is the tensile strength (ϵ_{max}), A is the activation energy, V is the activation volume, T is the temperature, R is the universal gas constant (8.31 J.mol⁻¹.K⁻¹). The correlation between σ and the logarithm of the Deformation Speed is linear, whose slope of the generated line, can be represented by Equation 2^[32]. The tensile strength (σ) was determined at three different deformation speeds (20, 50 and 100 mm/min) at temperature of 25 °C. The Izod Impact Resistance tests were performed on Pendulum Impact Testers, (HIT50P model) from ZwickRoell GmbH & Co, specimen 3.17 x 12.7 mm, notched, pendulum: 2.75 J and velocity 3.46 m/s^[33,34].

3. Results and Discussion

As shown in Figure 3a, the CaCO₃ microparticulates presented itself in the form of flakes with medium size of ~1.5 μm . Figure 3c, presents the CaCO₃ nanoparticulates micrograph with spherical shapes with size of ~70 nm. The histograms in Figures 3b, d show the size distributions of the respective CaCO₃ particles. Comparing the smallest microparticles to the largest nanoparticles reveals a relative

Table 2. Results of the characterization of concentrates and SME used.

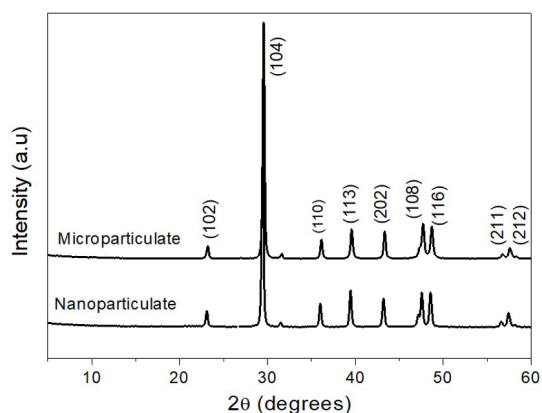
Sample	N (rpm)	Q (kg/h)	ϕ (μm)	Ash Content (%)	X_c (%)	Torque (%)	SME (kWh/kg)
hPP	-	-	-	0.15 \pm 0.01	65.9	-	-
M_250_10	250	10	1.7	21.19 \pm 0.41	63.6	69.8	0.12
M_250_15	250	15	1.7	18.88 \pm 0.26	54.5	78.4	0.09
M_500_10	500	10	1.7	20.17 \pm 0.10	59.7	58.6	0.20
M_500_15	500	15	1.7	20.27 \pm 0.06	63.2	65.8	0.15
N_250_10	250	10	0.04	20.14 \pm 0.02	61.5	73.3	0.12
N_250_15	250	15	0.04	19.68 \pm 0.10	59.7	80.7	0.09
N_500_10	500	10	0.04	17.16 \pm 0.14	57.3	62.4	0.21
N_500_15	500	15	0.04	18.66 \pm 0.06	63.6	66.4	0.15

**Figure 3.** Microscopy: (a) microparticulates CaCO_3 – 30,000x and (c) nanoparticles CaCO_3 – 75,790x in different magnification. Particle size distribution: (b) microparticulates and (d) nanoparticles.

size distribution difference of about 4x. Considering the D_{50} value, this relative distribution difference increases to about 20x. A similar distribution between the CaCO_3 micro and nanoparticles also was observed by Thio et al.^[16]

Regarding the diffraction patterns of the micro and nanoparticle CaCO_3 samples shown in Figure 4, the main diffraction peaks in 2θ can be observed at 23.2°, 29.6°, 36.3°, 39.6°, 43.3°, 47.7°, 48.6°, 56.6° and 57.6° characteristics of the crystallographic planes (102), (104), (110), (113), (202), (108), (116), (211) and (212) respectively in different phases of CaCO_3 ^[35].

The specific surface area (BET) of CaCO_3 particles, the nanoparticles presented value of $24.19 \pm 0.18 \text{ m}^2/\text{g}$, while the microparticles had a value of $6.89 \pm 0.16 \text{ m}^2/\text{g}$. These values differ from those reported by the manufacturers, likely due

**Figure 4.** X-ray diffractogram of micro and nanoparticle CaCO_3 .

to the interference of the surface treatment on the particles. Despite the nominal value being 20.0%, the obtained results closely matched as expected, except for sample N_500_10, which was 2.8 points below the nominal value, likely due to processing losses. However, this discrepancy didn't affect the results, as the studies were based on the actual sample values rather than the nominal ones. Important information from the X-ray diffraction test (range: 1 to 30°) enabled the identification of fillers and determination of the degree of crystallinity in the concentrate samples. Figures 5a-b display the diffractogram for the nano and microparticulate CaCO₃ concentrates, with characteristic peaks at 23.2° and 29.6°, confirming its presence^[35], which are characteristic of planes (102) and (104) respectively, as also observed in the diffractogram in Figure 04.

However, it is important to mention the presence of an important signal of 2θ = 16.0° related to the (300) plane, characteristic of the formation of the β phase of PP as also observed by Sakahara et al.^[36]. According to these authors, the increase in the intensity of the β phase in PP positively interferes in different mechanical properties, such as tensile strength, flexural modulus and impact resistance. This feature is explained by the tenacity of the beta crystalline phase and its metastability, which allows its conversion to the most common α crystalline phase observed under mechanical

load and thermal stress^[36]. In this study, it was found that the intensities of this 2θ = 16.0° peak are more intense for the PP/CaCO₃ nanocomposites, which had a positive impact on its mechanical properties, as will be discussed later. The ratio between these two areas results in the crystallinity degree (Xc), as shown in Equation 3^[36,37]. Figure 6 shows a treatment example applied to the hPP diffractogram, both with and without the amorphous halo, and the concentrate results are presented in Table 2.

$$X_c = \frac{A_c}{A_c + A_a} \tag{3}$$

The Xc results, is consistent with literature values, which range between 60 and 70%^[38]. For the concentrates, lower values are observed, possibly due to the high CaCO₃ content interfering with crystallite formation and growth. Using the extrusion parameters shown in Table 1, it was possible to determine and modulate the SME of the process according to extruder screw rotation (N) and extruder feed flow (Q)^[14]. The parameters associated are presented in Equation 4^[12,13]

$$SME = \left(\frac{\frac{N_0}{N_{max}} \times W_{max} \times \frac{T}{100}}{Q} \right) \tag{4}$$

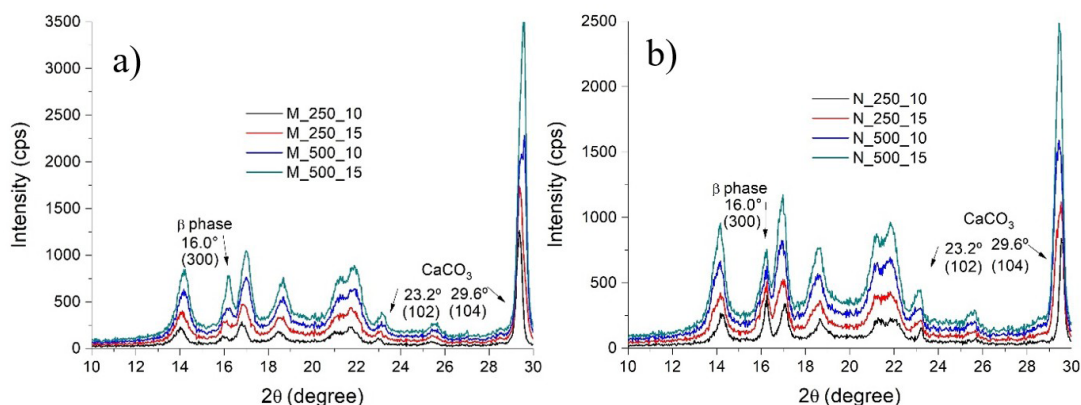


Figure 5. X-ray diffractogram of micro (a) and nanoparticle (b) CaCO₃ concentrate.

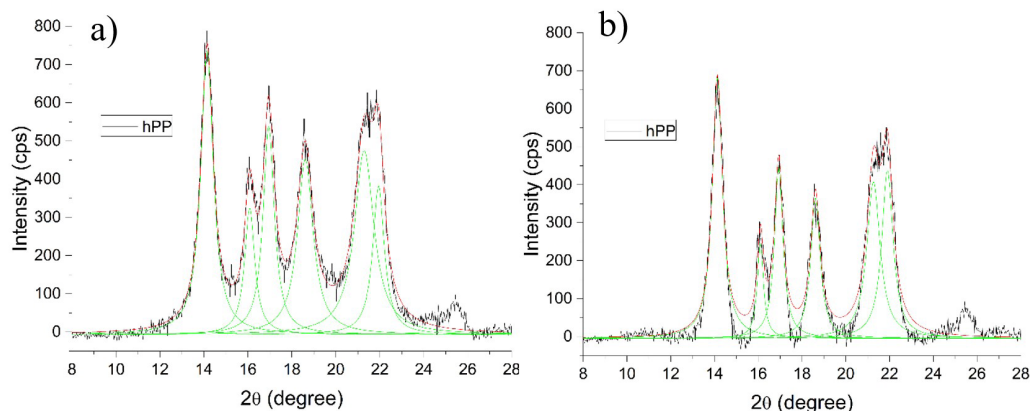


Figure 6. X-ray diffractogram of hPP with amorphous halo (a) and without amorphous halo (b).

Here, N_0 is the extruder screw rotation (rpm), N_{max} is the maximum extruder screw rotation (rpm), W_{max} is the maximum power of the extruder engine (kW), T is the extruder torque (%), and Q is the feed flow (kg/h). The SME values are shown in Table 2.

The compounds prepared with different SME levels did not show significant differences in X_c , likely due to the high mineral filler concentration. Specific conditions can favor or hinder the degree of crystallinity. Higher screw rotations combined with lower feed flows can provide more energy to the system, enhancing particle dispersion in the polymer matrix, particularly for smaller particles that are more difficult to disperse due to their high surface area^[12,15]. The composites inorganic material content was determined, considering the raw material purity. The actual $CaCO_3$ content in each sample was used, as shown in Tables 3, to minimize concentration effects. It was observed that the $CaCO_3$ content in the composites was very close to the nominal values, indicating minimal losses during processing.

Samples prepared with a feed flow of 10 kg/h showed equivalent values for both nano and microparticles. At 15 kg/h, microparticles performed better at a screw rotation of 250 rpm, while nanoparticles performed better at 500 rpm. Regarding

$CaCO_3$ content, microparticles showed stable properties with increasing filler content. However, nanocomposites exhibited an increasing tendency in impact resistance with increasing filler content, as depicted in Figure 7. As studied by Yang et al.^[4], Huang et al.^[9] and Eiras^[19], the addition of nanoparticulate $CaCO_3$ increases the composite impact resistance, in relation to original polymer.

Regarding mechanical properties under tension, the Young's Modulus, Tensile Strength (F_{max}), and Strain (F_{max}), were studied. For Young's Modulus, the microparticulate showed superior results at 250 rpm, while the nanoparticulate performed better at 500 rpm. The best results for both were achieved with a feed rate (Q) of 10 kg/h, as seen in Figure 8. However, these results are below those reported in the literature^[4,9,39].

In terms of Tensile Strength (F_{max}), all configurations exhibited better results for nanoparticles, particularly the sample processed at 500 rpm and 10 kg/h, showed superior properties compared to others, as depicted in Figure 9 and consistent with Yang et al.^[4]

For the strain (F_{max}) property, with 500 rpm exhibited higher deformation values, particularly when fed at 10 kg/h,

Table 3. $CaCO_3$ content for micro and nanocomposite

Sample	Ash content (%)	$CaCO_3$ content (%)	Sample	Ash content (%)	$CaCO_3$ content (%)
M_250_10_0.50	0.56 ± 0.01	0.55	N_250_10_0.50	0.60 ± 0.02	0.57
M_250_10_1.50	1.07 ± 0.04	1.04	N_250_10_1.50	1.54 ± 0.05	1.45
M_250_10_5.00	5.27 ± 0.07	5.14	N_250_10_5.00	4.96 ± 0.07	4.69
M_250_10_10.0	10.68 ± 0.19	10.41	N_250_10_10.0	10.16 ± 0.11	9.60
M_250_15_0.50	0.57 ± 0.01	0.56	N_250_15_0.50	0.57 ± 0.06	0.54
M_250_15_1.50	1.55 ± 0.08	1.51	N_250_15_1.50	1.56 ± 0.01	1.47
M_250_15_5.00	5.08 ± 0.11	4.95	N_250_15_5.00	5.05 ± 0.16	4.77
M_250_15_10.0	9.87 ± 0.17	9.62	N_250_15_10.0	9.97 ± 0.10	9.25
M_500_10_0.50	0.64 ± 0.06	0.62	N_500_10_0.50	0.51 ± 0.04	0.48
M_500_10_1.50	1.55 ± 0.10	1.51	N_500_10_1.50	1.31 ± 0.02	1.24
M_500_10_5.00	5.17 ± 0.07	5.04	N_500_10_5.00	4.36 ± 0.04	4.12
M_500_10_10.0	10.33 ± 0.03	10.07	N_500_10_10.0	8.33 ± 0.09	7.87
M_500_15_0.50	0.67 ± 0.04	0.65	N_500_15_0.50	0.54 ± 0.01	0.51
M_500_15_1.50	1.68 ± 0.09	1.64	N_500_15_1.50	1.50 ± 0.02	1.42
M_500_15_5.00	5.32 ± 0.03	5.19	N_500_15_5.00	5.06 ± 0.07	4.78
M_500_15_10.0	10.19 ± 0.18	9.94	N_500_15_10.0	9.63 ± 0.06	9.11

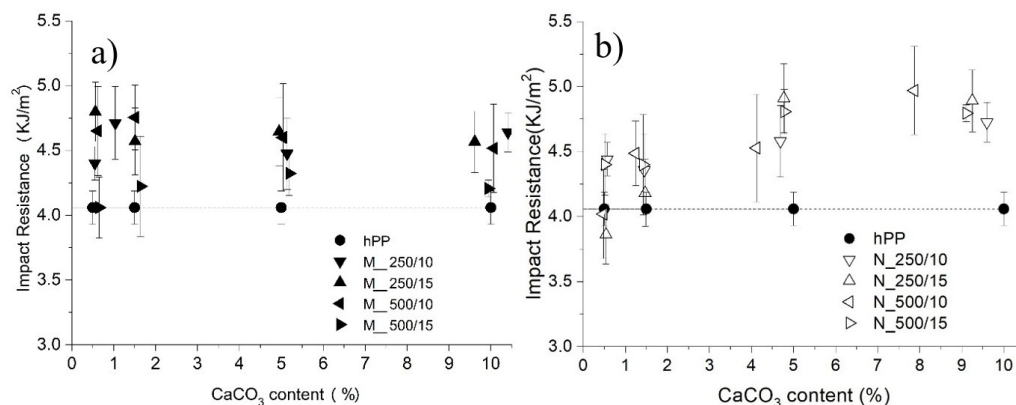


Figure 7. Impact resistance for microparticulated (a) and nanoparticulated composite (b).

where the highest SME (0.21 kWh/kg) was observed. In other conditions, the values between micro and nanoparticulated composites were similar. Analyzing the influence of particle size (ϕ), in microparticles, there is a strong tendency to reduce the strain increasing CaCO₃ content, but less pronounced for nano, as Figure 10.

The Activation Volume (V), determined by the *Eyring* equation, reflects the polymer-filler interface mobility. A smaller activation volume indicates greater restriction on the

mobility of the chain segments, suggesting better dispersion and interaction between the filler and the matrix. Using Equation 2 and the values of σ at different speeds^[22] for each composition, the V of the composites, was determined^[23,40] based on filler content, as shown in Figure 11.

The Activation Volume was indirectly measured by the Tensile Resistance (F_{max}), where it can observe that the results obtained are consistent with those reported by Rocha et al.^[15]. Higher rotations, coupled with lower feed flow, increase the

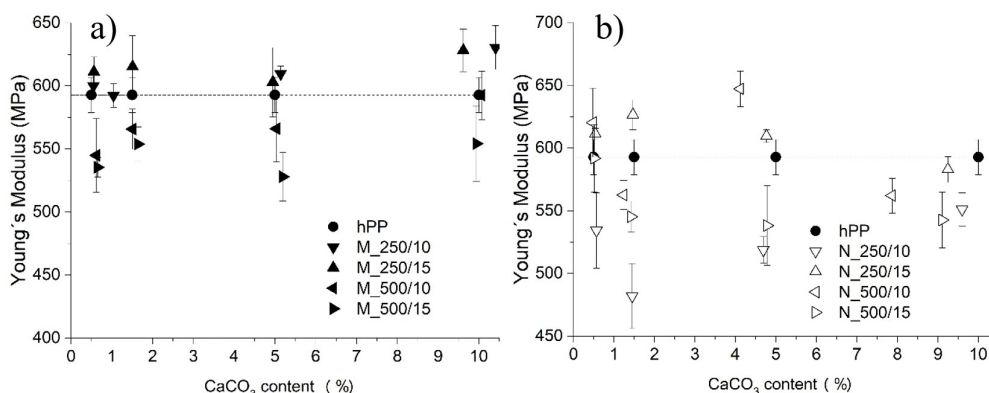


Figure 8. Young's Modulus under tensile for microparticulated (a) and nanoparticulated composite (b).

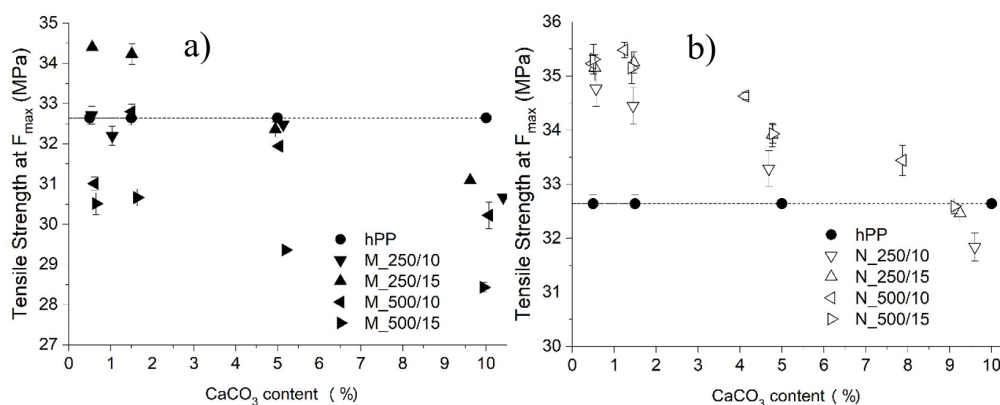


Figure 9. Tensile Strength (F_{max}) for microparticulated (a) and nanoparticulated composite (b).

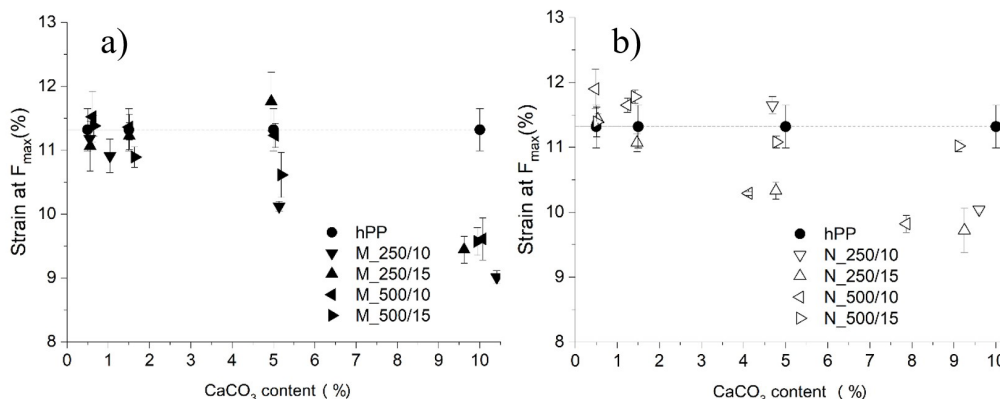


Figure 10. Strain (F_{max}) for microparticulate (a) and nanoparticulated composite (b).

SME used in the extrusion process, leading to better particle dispersion. This, in turn, enhances the mechanical properties of the composite due to increased surface interaction, as evidenced by the activation volume^[12]. The best composite formulations M_500_10 and N_500_10, with different wt% of micro and nanoparticulate CaCO₃ were investigated by SEM, after cryogenic fracture. Micrographs are shown in

Figures 12, revealing the CaCO₃ different morphology in the polymeric matrix. At 0.15wt% content of both micro (a1) and nanocomposite (a2) displayed effective dispersion, although with larger micrometric particles. At 1.50wt%, better dispersion of nanometric particles (b2) was observed compared to the microcomposite (b1). The same was observed at 5.00 wt%

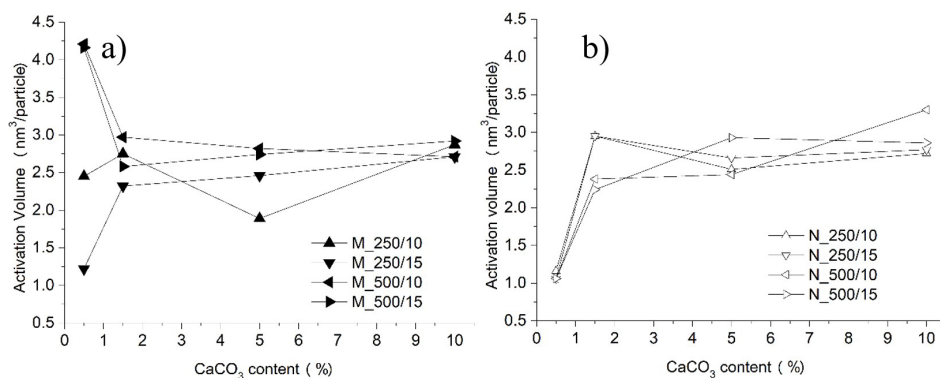


Figure 11. Activation volume for microparticulated (a) and nanoparticulated composite (b).

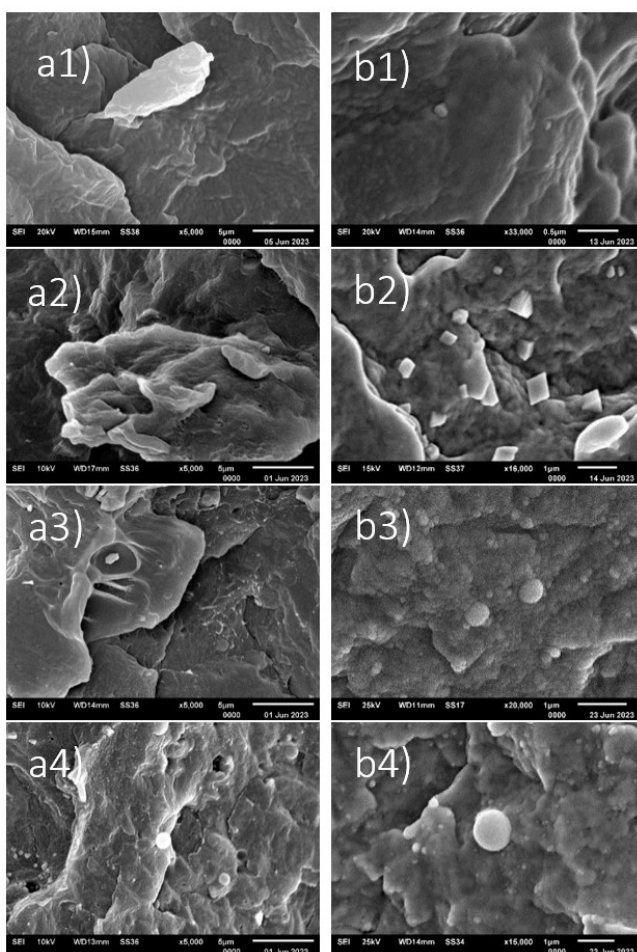


Figure 12. Micrographs of micro (a) and nanoparticulated composite (b) with 0.15% (1), 1.50% (2), 5.00% (3) and 10.00% (4) of CaCO₃ in different magnification.

(c), with good dispersion and distribution of particles in the nanocomposite (c2), with few agglomerates. Finally, at 10.00% (d), good particles distribution was observed in the nanocomposite (d2) with few agglomerates, which is indicative of efficiency in the dispersion process and potentially better particle-matrix adhesion compared to the microcomposite (d1). As is known, the higher level of agglomerates indicates poor dispersion and a lower level of reinforcement. Our mechanical results correlated with the microscopy images are quite consistent with the mechanical properties, as also observed previously by Yang et al.^[4] and Thio et al.^[16].

Based on the results from Impact, Tensile Strength, and Activation Volume, along with the micrographs, the condition: extruder screw rotation of 500 rpm and feed of 10 kg/h, exhibited the most favorable properties balance, credited to the higher SME utilized in the dispersion process (0.21 kWh/kg). Subsequent tests will be performed using these parameters (M_500_10 and N_500_10), with the outcomes detailed in Second Part of this study.

4. Conclusion

The study identified the processing condition with superior filler dispersion with Q:10 kg/h and N: 500 rpm. Under these conditions, the nanocomposite presented Young's Modulus with 4.12wt% increased by 9.2% compared to the hPP. The tensile strength (F_{max}) increased by 7.9% with just 0.48wt% of nanoparticulate CaCO₃, compared to hPP. Deformation (F_{max}) values remained similar for nano and microcomposites, with a notable increase of 5.1% for the 0.48wt% nanoparticle content compared to hPP. The nanocomposites with 0.48wt% and 1.24wt% stood out due to their smaller Activation Volume, compared to microparticles at the same content. The impact resistance of nanocomposite, increased by 22.4% compared to hPP, with 7.9wt%. Based on these results, it was determined the most favorable process parameters for achieving superior mechanical properties for the studied PP/CaCO₃ composites. The increase in the intensity of the beta phase diffraction peak for the CaCO₃ nanocomposites positively influenced the improvement of its mechanical properties in relation to the pure polymer and the microcomposites. However, it is advisable to explore other additional properties, such as thermal and barrier, using these parameters already determined for these systems. Furthermore, it is also necessary to investigate the influence of the D₅₀ filler content on the mechanical and thermal behavior at different wt% in PP. This type of investigation will be better explored in future work.

5. Author's Contribution

- **Conceptualization** – Juliano Martins Barbosa; Caroline Valadão Pacheco; Gisele Szilágyi; Patrícia Candioto de Oliveira; Renato Meneghetti Peres; Hélio Ribeiro.
- **Data curation** – Juliano Martins Barbosa; Hélio Ribeiro.
- **Formal analysis** – Juliano Martins Barbosa; Caroline Valadão Pacheco; Gisele Szilágyi; Patrícia Candioto de Oliveira; Renato Meneghetti Peres; Hélio Ribeiro.
- **Funding acquisition** – NA.
- **Investigation** – Juliano Martins Barbosa; Hélio Ribeiro.
- **Methodology** – Juliano Martins Barbosa; Hélio Ribeiro.
- **Project administration** – Juliano Martins Barbosa; Hélio Ribeiro.
- **Resources** – Juliano Martins Barbosa; Caroline Valadão Pacheco; Gisele Szilágyi; Patrícia Candioto de Oliveira; Renato Meneghetti Peres; Hélio Ribeiro.
- **Software** – NA.
- **Supervision** – Juliano Martins Barbosa; Hélio Ribeiro.
- **Validation** – Juliano Martins Barbosa; Caroline Valadão Pacheco; Gisele Szilágyi; Patrícia Candioto de Oliveira; Renato Meneghetti Peres; Hélio Ribeiro.
- **Visualization** – Juliano Martins Barbosa; Hélio Ribeiro.
- **Writing – original draft** – Juliano Martins Barbosa; Gisele Szilágyi; Hélio Ribeiro.
- **Writing – review & editing** – Juliano Martins Barbosa; Hélio Ribeiro.

6. Acknowledgements

This study received partial funding from the Coordenação de Aperfeiçoamento de Pessoal de Nível Superior - Brasil (CAPES) - Finance Code 001. The authors acknowledge the Materials Engineering Department of Mackenzie Presbyterian University (MACKENZIE), the Materials Engineering Department (DEMa) and the Graduate Program in Materials Science and Engineering (PPGCEM) of the Federal University of São Carlos (UFSCar), ZwickRoell do Brasil and Cromex S/A for their technical support and donation of raw materials.

7. References

1. Padilha, A. F. (2000). *Materiais de engenharia – microestrutura e propriedades*. São Paulo: Editora Hemus.
2. Callister, W. D. (2002). *Ciência e engenharia dos materiais: uma introdução*. Barueri: Editora LTC.
3. Wypych, G. (1999). *Handbook of fillers*. New York: Plastics Design Library.
4. Yang, K., Yang, Q., Li, G., Sun, Y., & Feng, D. (2006). Morphology and mechanical properties of polypropylene/calcium carbonate nanocomposites. *Materials Letters*, 60(6), 805-809. <http://doi.org/10.1016/j.matlet.2005.10.020>.
5. Rabelo, M. (2000). *Adivição de polímeros*. São Paulo: Artliber Editora.
6. Fischer, H. (2003). Polymer nanocomposite: from fundamental research to specific application. *Materials Science and Engineering C*, 23(6-8), 763-772. <http://doi.org/10.1016/j.msec.2003.09.148>.
7. Rodolfo, A., Nunes, L. R., & Ormanji, W. (2006). *Tecnologia do PVC*. São Paulo: ProEditores/Braskem. Retrieved in 2024, May 19, from https://www.braskem.com/Portal/Principal/Arquivos/Download/Upload/Tecnologia%20do%20PVC%202a%20edi%C3%A7%C3%A3o_22.pdf
8. Mai, Y.-W., & Yu, Z.-Z. (Eds.) (2006). *Polymer nanocomposites*. Cambridge, England: Woodhead Publishing Limited. <http://doi.org/10.1533/9781845691127>.
9. Huang, Z., Lin, Z., Cai, Z., & Mai, K. (2004). Physical and mechanical properties of nano-CaCO₃/PP composites modified with acrylic acid. *Plastics, Rubber and Composites*, 33(8), 343-351. <http://doi.org/10.1179/174328904X22314>.

10. Ribeiro, H., Silva, W. M., Neves, J. C., Calado, H. D. R., Paniago, R., Seara, L. M., Camarano, D. M., & Silva, G. G. (2015). Multifunctional nanocomposites based on tetraethylenepentamine-modified graphene oxide/epoxy. *Polymer Testing*, *43*, 182-192. <http://doi.org/10.1016/j.polymertesting.2015.03.010>.
11. Barbosa, J. M. (2021). *Influência da incorporação de negro de fumo e carbonato de cálcio micro e nanoparticulado nas propriedades reológicas, colorimétricas e mecânicas de filmes de polietileno de baixa densidade* (Doctoral dissertation). Universidade Federal de São Carlos, São Carlos.
12. Domenech, T., Peuvrel-Disdier, E., & Vergnes, B. (2013). The importance of specific mechanical energy during twin screw extrusion of organoclay based polypropylene nanocomposites. *Composites Science and Technology*, *75*, 7-14. <http://doi.org/10.1016/j.compscitech.2012.11.016>.
13. Century Extrusion Group. (2018). *Torque vs Specific Energy*. *Process Technology* [Webinar]. Century Extrusion Group. Retrieved in 2024, January 13, from <https://ekc.cpmextrusiongroup.com/project/torque-vs-specific-energy/>
14. Barbosa, J. M., Beatrice, C. A. G., & Pessan, L. A. (2022). Influence of carbon black trimodal mixture on LDPE films properties: Part2 – SME. *Polímeros: Ciência e Tecnologia*, *32*(3), e2022030. <http://doi.org/10.1590/0104-1428.20220053>.
15. Rocha, M. C. G., Silva, A. H. F. T., Coutinho, F. M. B., & Silva, A. L. N. (2005). Study of composites based on polypropylene and calcium carbonate by experimental design. *Polymer Testing*, *24*(8), 1049-1053. <http://doi.org/10.1016/j.polymertesting.2005.05.008>.
16. Thio, Y. S., Argon, A. S., Cohen, R. E., & Weinberg, M. (2002). Toughening of Isotactic polypropylene with CaCO₃ particles. *Polymers*, *43*(13), 3661-3674. [http://doi.org/10.1016/S0032-3861\(02\)00193-3](http://doi.org/10.1016/S0032-3861(02)00193-3).
17. Chan, C.-M., Wu, J., Li, J.-X., & Cheung, Y.-K. (2002). Polypropylene/ Calcium carbonate nanocomposite. *Polymer*, *43*(10), 2981-2992. [http://doi.org/10.1016/S0032-3861\(02\)00120-9](http://doi.org/10.1016/S0032-3861(02)00120-9).
18. Zhang, Q.-X., Yu, Z.-Z., Xie, X.-L., & Mai, Y.-W. (2004). Crystallization and Impact energy of Polypropylene/CaCO₃ nanocomposite with nonionic modifier. *Polymer*, *45*(17), 5985-5994. <http://doi.org/10.1016/j.polymer.2004.06.044>.
19. Eiras, D. (2009). *Tenacificação de polipropileno com nanopartículas de carbonato de cálcio* (Master's thesis). Universidade Federal de São Carlos, São Carlos.
20. Silva, A. L. N., Bertolino, L. C., Nasser, R. O., Costa, L. S., Melo, A. A., Marquezine, L. P. S., Silva, A. H. M. F. T., Alves, V. O., & Nascimento, C. R. V. (2013). Application of a factorial planning for the evaluation of mechanical, thermal, morphologic and flow properties of PEAD and CaCO₃ composites. *Matéria (Rio de Janeiro)*, *18*(3), 1382-1394. <http://doi.org/10.1590/S1517-70762013000300006>.
21. Barbosa, J. M., Beatrice, C. A. G., & Pessan, L. A. (2022). Influence of carbon black trimodal mixture on LDPE films properties: Part1 – DOE. *Polímeros: Ciência e Tecnologia*, *32*(3), e2022029. <http://doi.org/10.1590/0104-1428.20220039>.
22. Barbosa, J. M. (2011). *Estudo das propriedades mecânicas, térmicas e de transporte do compósito com carbonato de cálcio nano e microparticulado em polipropileno* (Master's thesis). Universidade Federal de São Carlos, São Carlos.
23. Barbosa, J. M., Pacheco, C. P., Szilágyi, G., Oliveira, P. C. M., Peres, R. M., & Ribeiro, H. (2022). *Mechanical properties of polypropylene/calcium carbonate micro and nanocomposites*. In *Anais do 17º Congresso Brasileiro de Polímeros – CBPol* (p.760). São Paulo: ABPol.
24. NanoMaterials Technology Pte Ltd. (2024). Retrieved in 2024, January 13, from <https://nanomt.com/products/nppcc/>
25. Omya International AG. (2023). Retrieved in 2023, December 20, from <https://www.omya.com/en/products/polymers>
26. Dow Inc. (2024) Retrieved in 2024, May 11, from <https://www.dow.com/pt-br/pdp.fusabond-p353-functional-polymer.1891762z.html#overview>
27. Braskem S/A. (2024). Retrieved in 2024, May 19, from <https://www.braskem.com/busca-de-produtos?p=309>
28. Lotti, C., Isaac, C. S., Branciforti, M. C., Alves, R. M. V., Liberman, S., & Bretas, R. E. S. (2008). Rheological, mechanical and transport property of blow films of high density polyethylene nanocompósitos. *European Polymer Journal*, *44*(5), 1346-1357. <http://doi.org/10.1016/j.eurpolymj.2008.02.014>.
29. American Society for Testing and Materials – ASTM. (2023). *ASTM D1238-23a: Standard Test Method for Melt Flow Rates of Thermoplastics by Extrusion Plastometer*. West Conshohocken: ASTM International. <http://doi.org/10.1520/D1238-23A>.
30. American Society for Testing and Materials – ASTM. (2022). *ASTM D5630-22: Standard Test Method for Ash Content in Plastics*. West Conshohocken: ASTM International. <http://doi.org/10.1520/D5630-22>.
31. American Society for Testing and Materials – ASTM. (2022). *ASTM D638-22: Standard Test Method for Tensile Properties of Plastics*. West Conshohocken: ASTM International. <http://doi.org/10.1520/D0638-22>.
32. Ward, I. M., & Pinnock, P. R. (1983). *Mechanical properties of solid polymers*. West Sussex: John Wiley and Sons.
33. Brown, R. (2002). *Handbook of polymer testing – short-term mechanical tests*. Shawburry: Rapra Technology.
34. American Society for Testing and Materials – ASTM. (2023). *ASTM D256-23e1: Standard Test Method for Determining the Izod Pendulum Impact Resistance of Plastics*. West Conshohocken: ASTM International. <http://doi.org/10.1520/D0256-23E01>.
35. Saraya, M. E.-S. I., & Rokbaa, H. H. A. L. (2016). Preparation of vaterite calcium carbonate in the form of spherical nano-size particles with the aid of polycarboxylate superplasticizer as a capping agent. *American Journal of Nanomaterials*, *4*(2), 44-51. <http://doi.org/10.12691/ajn-4-2-3>.
36. Sakahara, R., Lima, A., & Wang, S. H. (2014). Influence of the beta crystalline phase fraction on the mechanical behavior of polypropylene/calcium carbonate/polypropylene - graft - maleic anhydride composites. *Polímeros: Ciência e Tecnologia*, *24*(5), 554-560. <http://doi.org/10.1590/0104-1428.1692>.
37. Uzun, İ. (2023). Methods of determining the degree of crystallinity of polymers with X-ray diffraction. *Journal of Polymer Research*, *30*(10), 394. <http://doi.org/10.1007/s10965-023-03744-0>.
38. Canevarolo, S. V. (2004). *Técnicas de caracterização de polímeros*. São Paulo: Artliber Editora.
39. Mareri, P., Bastide, S., Binda, N., & Crespy, A. (1998). Mechanical behaviour of PP Composites containing fine mineral filler: effect of filler surface treatment. *Composites Science and Technology*, *58*(5), 747-752. [http://doi.org/10.1016/S0266-3538\(97\)00156-5](http://doi.org/10.1016/S0266-3538(97)00156-5).
40. Barbosa, J. M., & Ruvalo, A., Fo. (2009). *Estudo das propriedades mecânicas do nanocompósito e microcompósito de carbonato de cálcio em polipropileno*. In *Anais do 10º Congresso Brasileiro de Polímeros – CBPol* (p. 690). São Paulo: ABPol.

Received: July 03, 2024

Revised: Sept. 24, 2024

Accepted: Nov. 03, 2024